

# Lanthanide-doped inorganic nanoparticles turn molecular triplet excitons bright

<https://doi.org/10.1038/s41586-020-2932-2>

Received: 24 April 2019

Accepted: 23 September 2020

Published online: 25 November 2020

 Check for updates

Sanyang Han<sup>1,15</sup>, Renren Deng<sup>1,2,15</sup>✉, Qifei Gu<sup>1</sup>, Limeng Ni<sup>1</sup>, Uyen Huynh<sup>1</sup>, Jiangbin Zhang<sup>1,3,4</sup>, Zhigao Yi<sup>5</sup>, Baodan Zhao<sup>1,6</sup>, Hiroyuki Tamura<sup>7</sup>, Anton Pershin<sup>8</sup>, Hui Xu<sup>9</sup>, Zhiyuan Huang<sup>10</sup>, Shahab Ahmad<sup>11</sup>, Mojtaba Abdi-Jalebi<sup>1,12</sup>, Aditya Sadhanala<sup>1</sup>, Ming Lee Tang<sup>10</sup>, Artem Bakulin<sup>3</sup>, David Beljonne<sup>8</sup>, Xiaogang Liu<sup>5,13,14</sup>✉ & Akshay Rao<sup>15</sup>✉

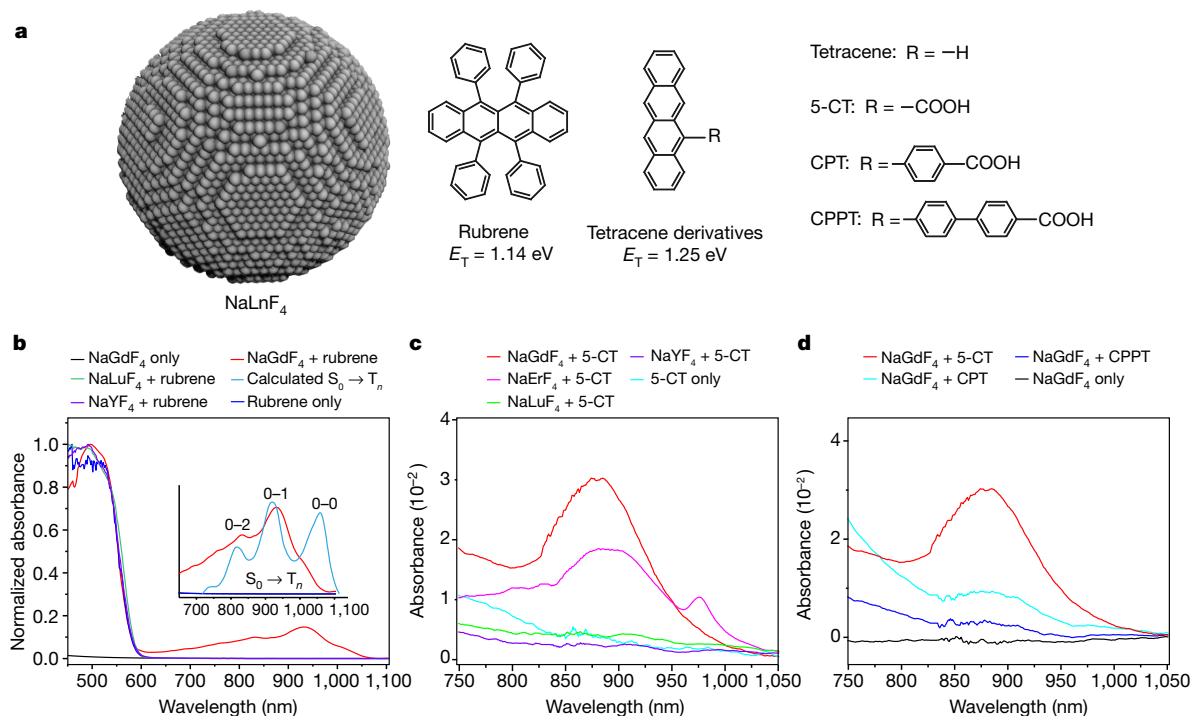
The generation, control and transfer of triplet excitons in molecular and hybrid systems is of great interest owing to their long lifetime and diffusion length in both solid-state and solution phase systems, and to their applications in light emission<sup>1</sup>, optoelectronics<sup>2,3</sup>, photon frequency conversion<sup>4,5</sup> and photocatalysis<sup>6,7</sup>. Molecular triplet excitons (bound electron–hole pairs) are ‘dark states’ because of the forbidden nature of the direct optical transition between the spin-zero ground state and the spin-one triplet levels<sup>8</sup>. Hence, triplet dynamics are conventionally controlled through heavy-metal-based spin–orbit coupling<sup>9–11</sup> or tuning of the singlet–triplet energy splitting<sup>12,13</sup> via molecular design. Both these methods place constraints on the range of properties that can be modified and the molecular structures that can be used. Here we demonstrate that it is possible to control triplet dynamics by coupling organic molecules to lanthanide-doped inorganic insulating nanoparticles. This allows the classically forbidden transitions from the ground-state singlet to excited-state triplets to gain oscillator strength, enabling triplets to be directly generated on molecules via photon absorption. Photogenerated singlet excitons can be converted to triplet excitons on sub-10-picosecond timescales with unity efficiency by intersystem crossing. Triplet exciton states of the molecules can undergo energy transfer to the lanthanide ions with unity efficiency, which allows us to achieve luminescent harvesting of the dark triplet excitons. Furthermore, we demonstrate that the triplet excitons generated in the lanthanide nanoparticle–molecule hybrid systems by near-infrared photoexcitation can undergo efficient upconversion via a lanthanide–triplet excitation fusion process: this process enables endothermic upconversion and allows efficient upconversion from near-infrared to visible frequencies in the solid state. These results provide a new way to control triplet excitons, which is essential for many fields of optoelectronic and biomedical research.

Figure 1a shows a schematic of the lanthanide (Ln)-doped nanoparticles (nanocrystals of NaLnF<sub>4</sub>) and the structures of some of the model molecules used in our study (rubrene and tetracene derivatives) along with their triplet energies. Unlike semiconductor quantum dots, these lanthanide-doped nanocrystals are insulators and their optoelectronic properties are governed solely by the lanthanide ions. We begin by preparing blended films of rubrene and NaGdF<sub>4</sub> nanocrystals by drop-casting (Supplementary Figs. 1 and 2).

Figure 1b shows the absorption spectra, measured by photothermal deflection spectroscopy (PDS), of a NaGdF<sub>4</sub>–rubrene blend film, a pristine rubrene film and a pure NaGdF<sub>4</sub> film. Apart from the typical absorption features associated with the S<sub>0</sub> → S<sub>n</sub> (ground-state singlet to excited-state singlets) transitions in rubrene, we observe new absorption features between 700 nm and 1,100 nm in the NaGdF<sub>4</sub>–rubrene blend film. By contrast, the pristine rubrene film and the NaGdF<sub>4</sub>-only film have no absorptions in the same region. The spectra reveal an

<sup>1</sup>Cavendish Laboratory, University of Cambridge, Cambridge, UK. <sup>2</sup>Institute for Composites Science Innovation, School of Materials Science and Engineering, Zhejiang University, Hangzhou, China. <sup>3</sup>Department of Chemistry, Imperial College London, London, UK. <sup>4</sup>College of Advanced Interdisciplinary Studies, National University of Defense Technology, Changsha, China.

<sup>5</sup>Department of Chemistry, National University of Singapore, Singapore, Singapore. <sup>6</sup>State Key Laboratory of Modern Optical Instrumentation, College of Optical Science and Engineering, International Research Center for Advanced Photonics, Zhejiang University, Hangzhou, China. <sup>7</sup>Department of Chemical System Engineering, The University of Tokyo, Tokyo, Japan. <sup>8</sup>Laboratory for Chemistry of Novel Materials, University of Mons, Mons, Belgium. <sup>9</sup>School of Chemistry and Material Science, Heilongjiang University, Harbin, China. <sup>10</sup>Department of Chemistry, University of California, Riverside, Riverside, CA, USA. <sup>11</sup>Advanced Energy Materials Group, Department of Physics, Indian Institute of Technology Jodhpur, Jodhpur, India. <sup>12</sup>Institute for Materials Discovery, University College London, London, UK. <sup>13</sup>The N.1 Institute for Health, National University of Singapore, Singapore, Singapore. <sup>14</sup>Joint School of National University of Singapore and Tianjin University, International Campus of Tianjin University, Fuzhou, China. <sup>15</sup>These authors contributed equally: Sanyang Han, Renren Deng. ✉e-mail: rdeng@zju.edu.cn; chmlx@nus.edu.sg; ar525@cam.ac.uk



**Fig. 1 | Lanthanide-nanocrystal-coupled triplet excitation.** **a**, Schematic illustration of a lanthanide-doped nanocrystal ( $\text{NaLnF}_4$ ) and the organic molecules in our study. Note that  $E_T$  refers to the triplet energy of the molecules. **b**, Comparison of the PDS spectra of films of  $\text{NaGdF}_4$ -rubrene,  $\text{NaLuF}_4$ -rubrene,  $\text{NaYF}_4$ -rubrene with pristine rubrene and with  $\text{NaGdF}_4$  only. Only the system in which the lanthanide has unpaired spin (that is, the  $\text{NaGdF}_4$ -rubrene films) shows a broadband absorption from 700 nm to 1,100 nm; the inset shows that this absorption matches the calculated direct transition from

the ground singlet state ( $S_0$ ) to the lowest triplet state ( $T_1$ ). **c**, Comparison of the absorption spectra of 5-CT coupled with various lanthanide nanoparticles, including  $\text{NaGdF}_4$ ,  $\text{NaErF}_4$ ,  $\text{NaLuF}_4$  and  $\text{NaYF}_4$ . Enhanced NIR absorption, related to the direct excitation of triplets, is only observed in the presence of lanthanide ions with unpaired spins ( $\text{Gd}^{3+}$  and  $\text{Er}^{3+}$ ). **d**, Comparison of absorption spectra of  $\text{NaGdF}_4$  nanocrystals coupled with tetracene derivatives (5-CT, CPT, CPPT). The enhanced NIR absorption decreases with increasing spacing between the lanthanide nanoparticle and the core of the molecule.

approximately 200-fold enhancement in the near-infrared (NIR) absorbance of the  $\text{NaGdF}_4$ -rubrene blend compared with the pristine rubrene film. To understand this observation, we performed density functional theory and multireference second-order Møller–Plesset perturbation theory calculations (see Supplementary Information section 2). We found that the experimentally measured absorption in the NIR region (800–1,100 nm) matches well with the calculated absorption for the  $S_0 \rightarrow T_1$  transition of an isolated rubrene molecule (Fig. 1b, inset). Note that the theoretical prediction for the  $S_0^v \rightarrow T_1^v$  ( $v-v=0-0$ , where  $v$  represents a vibronic state) transition shows a much higher intensity. We attributed this suppression of the 0-0 band to the Herzberg–Teller mechanism, as described previously<sup>14</sup>. The extra absorption in the  $\text{NaGdF}_4$ -rubrene blend film is thus assigned to the  $S_0 \rightarrow T_n$  transition of rubrene, implying that the usually dark  $S_0 \rightarrow T_n$  transition has become bright in the blended system. Similarly, the enhanced dark  $S_0 \rightarrow T_n$  transition feature was also observed in tetracene-derivative-based blends (Supplementary Fig. 3).

One explanation for the enhanced  $S_0 \rightarrow T_n$  absorption could be related to the spin–orbit coupling associated with the presence of heavy atoms (atomic number  $Z=64$  for Gd). To test this hypothesis, we prepared blended films of rubrene with different types of lanthanide-doped nanoparticles, including  $\text{NaGdF}_4$ ,  $\text{NaYF}_4$  and  $\text{NaLuF}_4$ .  $\text{Gd}^{3+}$  has seven unpaired  $4f$  electrons<sup>15</sup>, whereas  $\text{Y}^{3+}$  ( $Z=39$ ) and  $\text{Lu}^{3+}$  ( $Z=71$ ) have zero spin momentum (Supplementary Table 1). The absorption of the  $S_0 \rightarrow T_n$  transition was observed only in the blends with non-zero spin, while no features could be observed for the  $\text{Y}^{3+}$ - and  $\text{Lu}^{3+}$ -based blends despite the higher atomic mass of  $\text{Lu}^{3+}$  (Fig. 1b). These results suggest that the enhanced  $S_0 \rightarrow T_n$  transition is not due to the heavy-atom-induced spin–orbit coupling but related to the spins of unpaired  $4f$  electrons of lanthanide ions.

To further investigate the nature of the coupling between organic molecules and lanthanide nanocrystals, we prepared lanthanide nanoparticles modified with a series of carboxylic acid-functionalized tetracene derivatives, 5-carboxylic acid tetracene (5-CT), 4-(tetracen-5-yl)benzoic acid (CPT) and 4'-(tetracen-5-yl)-[1,1'-biphenyl]-4-carboxylic acid (CPPT), as shown in Fig. 1a. These molecules can selectively bind to surface cations of the nanocrystals through their carboxylic groups. The different spacer groups allow us to control the distance between lanthanide ions and the tetracene core, where the triplet excitons will be localized. We studied blended films of 5-CT with different  $\text{NaLnF}_4$  ( $\text{Ln} = \text{Gd}^{3+}$ ,  $\text{Er}^{3+}$ ,  $\text{Y}^{3+}$  or  $\text{Lu}^{3+}$ ) nanocrystals, as shown in Fig. 1c. The absorption spectra showed that all the lanthanides with unpaired  $4f$  electrons ( $\text{Gd}^{3+}$  and  $\text{Er}^{3+}$ ) give rise to an enhanced NIR absorption of 5-CT molecules, whereas the lanthanides without unpaired electrons ( $\text{Y}^{3+}$  and  $\text{Lu}^{3+}$ ) have a negligible effect. Figure 1d compares the effects of longer spacer groups. As we move from 5CT to CPT and CPPT, it was observed that the absorption in the NIR spectral region decreases. This result confirms that the coupling between lanthanides and tetracene molecules is very sensitive to the distance between them. On the basis of these observations, we propose that the proximity of the organic molecules to the lanthanide ions with unpaired spins permits photon absorption to directly generate triplet states,  $S_0 \rightarrow T_n$ . We return to the nature of this interaction later.

We next explore the effect of the lanthanide ions on the excited states of the organic semiconductors. We chose 9-[3-carboxyl-4-(diphenylphosphinoyl)phenyl]-9H-carbazole (CPPOA) as a model molecule owing to its high-lying triplet state (which will be important for the discussion of energy transfer below). We prepared colloidal solutions of  $\text{NaYF}_4@/\text{NaLnF}_4$  core-shell nanoparticles with surface-bound

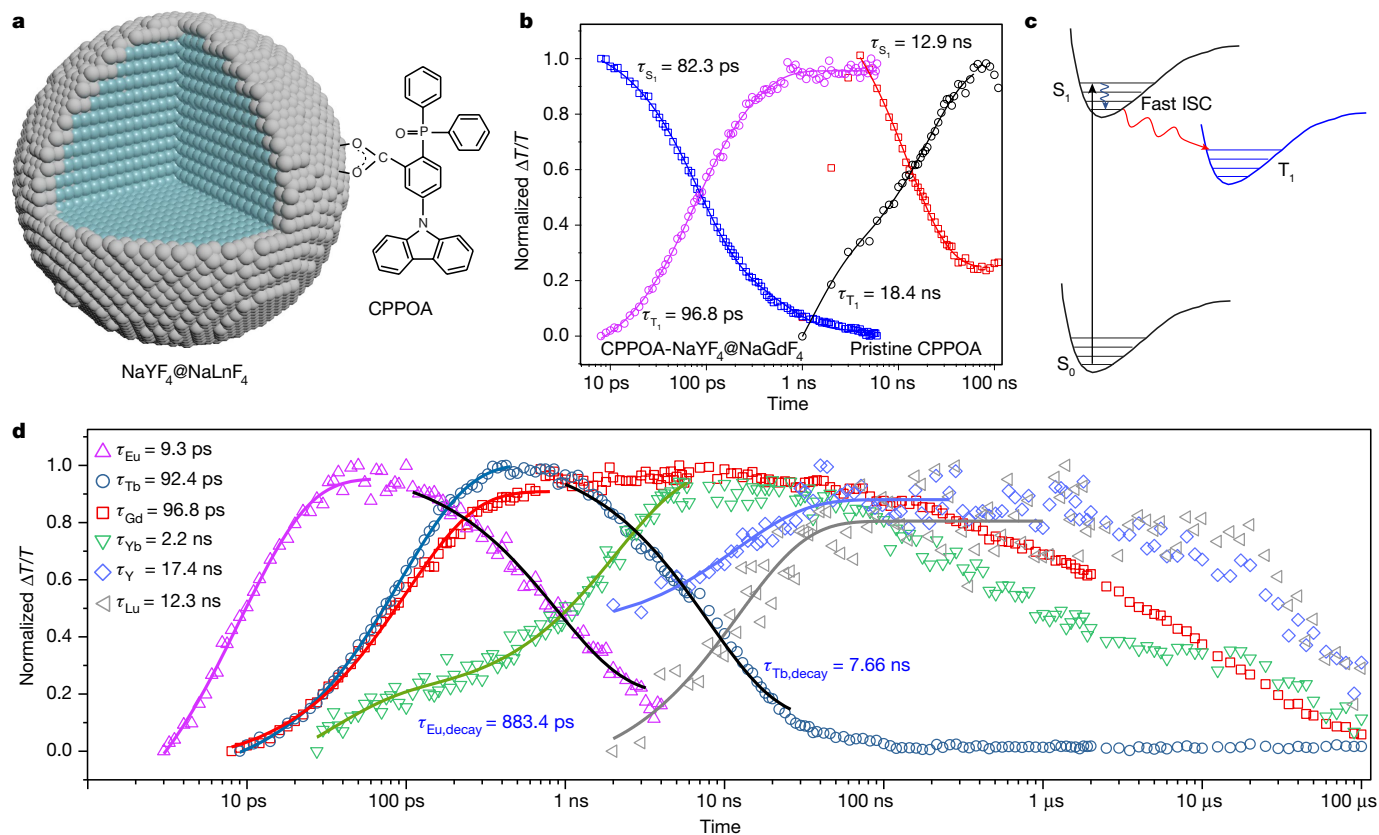


**Fig. 2 | Ultrafast intersystem crossing in organic molecules coupled to lanthanide-doped nanoparticles.** **a**, Schematic illustration of a  $\text{NaYF}_4@ \text{NaLnF}_4$  core-shell nanoparticle modified with CPPOA. **b**, Extracted kinetics showing the singlet ( $S_1$ ) decay and triplet ( $T_1$ ) growth of a solution containing pristine CPPOA molecules and of a solution of CPPOA-modified  $\text{NaYF}_4@ \text{NaGdF}_4$  nanoparticles. The singlet lifetime decreases from 12.9 ns in the pristine CPPOA to 82.3 ps in CPPOA-modified  $\text{NaYF}_4@ \text{NaGdF}_4$ , indicating greatly enhanced intersystem crossing (ISC). Note that  $\Delta T/T$  refers to the fractional differential transmission signal of the probe in transient absorption spectra. **c**, The interaction between the lanthanides and the molecules accelerates the ISC from the singlet to triplet exciton states of the molecule.

CPPOA molecules (Fig. 2a) and studied the dynamics of photoexcitations using pump-probe spectroscopy. The  $S_1$  state of CPPOA on the  $\text{NaYF}_4@ \text{NaGdF}_4$  nanoparticle was found to decay with a time constant of 82 ps (Fig. 2b), concomitant with the rise time of the triplet excitons ( $T_1$ , 97 ps). This indicates that the photogenerated singlet of CPPOA attached to the  $\text{NaYF}_4@ \text{NaGdF}_4$  nanoparticles undergoes rapid intersystem crossing (ISC). By contrast, the singlet of the pristine CPPOA shows a decay time of 12.9 ns with a concomitant triplet rise over 18.4 ns. Thus, the presence of the  $\text{Gd}^{3+}$ -based nanoparticles increases the rate of the ISC by three orders of magnitude (Fig. 2c). To investigate this further, we attached CPPOA to a series of  $\text{NaYF}_4@ \text{NaLnF}_4$  core-shell nanoparticles with different lanthanide ions in the shell and measured the triplet generation rate. As shown in Fig. 2d, we observe an enhanced ISC rate for nanoparticles with unpaired 4f electrons ( $\text{Tb}^{3+}$ ,  $\text{Eu}^{3+}$ ,  $\text{Gd}^{3+}$  and  $\text{Yb}^{3+}$ ), but not for those with no unpaired spins ( $\text{Y}^{3+}$  and  $\text{Lu}^{3+}$ ) (Supplementary Tables 1–3). The same trend was observed in sub-gap absorption enhancement for CPPOA-capped nanoparticles, analogous to the results in Fig. 1 (Supplementary Figs. 9 and 10a). For  $\text{Eu}^{3+}$ -doped nanoparticles, we measured a triplet rise time of 9.3 ps, which is 1,978 times faster than that of the pristine CPPOA molecules. The ISC efficiency is estimated to be 99.4%, based on the singlet lifetime quenching. Thus, in addition to turning  $S_0 \rightarrow T_n$  transitions bright, the interaction between

**d**, Kinetics of triplet generation and decay in CPPOA molecules attached to different types of core-shell nanoparticles. The compositions of the core-shell nanoparticles are  $\text{NaYF}_4@ \text{NaEuF}_4$ ,  $\text{NaYF}_4@ \text{NaGdF}_4$ ,  $\text{NaYF}_4@ \text{NaTbF}_4$ ,  $\text{NaYF}_4@ \text{NaYbF}_4$ ,  $\text{NaYF}_4@ \text{NaLuF}_4$  and  $\text{NaYF}_4@ \text{NaYF}_4$ . The key at top left gives the fitted values of  $\tau_{T_n}$  for the increasing part of each curve. For lanthanides with unpaired 4f electrons ( $\text{Tb}^{3+}$ ,  $\text{Eu}^{3+}$ ,  $\text{Gd}^{3+}$  and  $\text{Yb}^{3+}$ ) enhanced ISC is seen, whereas those with no unpaired spins ( $\text{Y}^{3+}$  and  $\text{Lu}^{3+}$ ) show no obvious enhancement in ISC. An enhanced triplet decay ( $\tau_{T_1, \text{decay}} = 7.66$  ns and  $\tau_{\text{Eu, decay}} = 883$  ps) of CPPOA on the nanoparticles containing  $\text{Tb}^{3+}$  or  $\text{Eu}^{3+}$  suggests triplet energy transfer to the lanthanide ions.

the CPPOA and the unpaired spins on the lanthanide nanoparticles also yields highly efficient ISC (ref. 16; see Supplementary Figs. 11–32 for full details).

It can be seen in Fig. 2d that the fast rise of the  $T_1$  state for  $\text{Tb}^{3+}$ - and  $\text{Eu}^{3+}$ -containing nanoparticles is accompanied by a quick decay of that state (7.66 ns for  $\text{Tb}^{3+}$  and 883 ps for  $\text{Eu}^{3+}$ ). This decay is caused by the energy transfer of the  $T_1$  state from CPPOA to the  $^5D_1/^5D_0$  and  $^5D_4$  levels of  $\text{Eu}^{3+}$  and  $\text{Tb}^{3+}$ , respectively (Fig. 3a). On the basis of the quenching of the triplet lifetime, the calculated quantum efficiency of triplet energy transfer from CPPOA to lanthanide nanoparticles exceeds 99%. This near-quantitative triplet energy transfer gives rise to bright luminescence from the lanthanide ions on excitation of the coupled systems at 365 nm (Fig. 3b and Supplementary Figs. 10b, 33–35). These results show that molecular triplet excitons can be efficiently transferred to lanthanide-doped nanoparticles, allowing the luminescent harvesting of normally dark triplet excitons.

This luminescent harvesting of triplet excitons is not restricted to triplets generated by ISC on the surface of the nanoparticles but is also relevant for triplets generated by other processes such as singlet fission. Tetracene and rubrene are both well-known singlet fission materials, in which the photogenerated singlet excitons rapidly and efficiently convert to a pair of triplet excitons<sup>13,17</sup>. Figure 3c shows data for blend films of tetracene and rubrene with  $\text{NaGdF}_4: \text{Yb}$  (50 mol%)

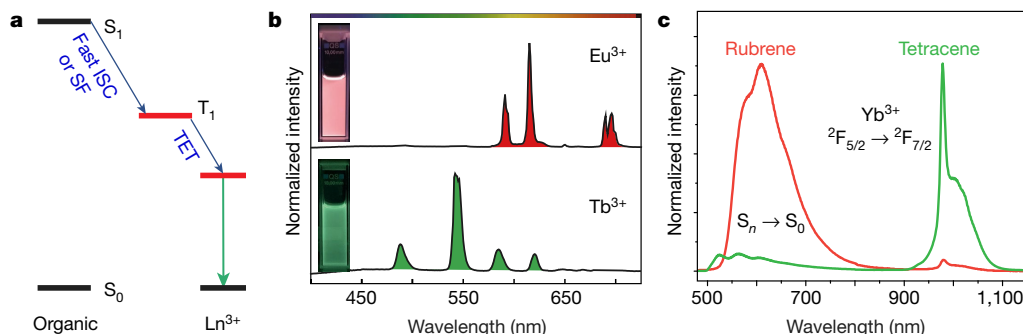


**Fig. 3 | Triplet energy transfer from molecules to nanoparticles.**

**a**, Simplified energy diagram showing triplet energy transfer (TET) from the molecular triplet state to lanthanide emitters ( $\text{Ln}^{3+}$ ) following a fast intersystem crossing (ISC) or singlet fission (SF) process. **b**, Photoluminescence spectra and corresponding luminescence photographs of colloidal solutions containing CPPOA-modified  $\text{NaYF}_4@/\text{NaEuF}_4$  nanoparticles (top) and CPPOA-modified  $\text{NaYF}_4@/\text{NaTbF}_4$  nanoparticles (bottom) under excitation at

365 nm. **c**, Photoluminescence spectra of  $\text{NaGdF}_4:\text{Yb}$ -tetracene blend (green curve) and  $\text{NaGdF}_4:\text{Yb}$ -rubrene blend (red curve) films excited at 405 nm. Luminescence arises from the transfer of triplet excitons generated via singlet fission to the  ${}^2\text{F}_{5/2} \rightarrow {}^2\text{F}_{7/2}$  transition of  $\text{Yb}^{3+}$ . The process is inefficient in rubrene owing to its triplet energy being lower than the  ${}^2\text{F}_{5/2} \rightarrow {}^2\text{F}_{7/2}$  transition of  $\text{Yb}^{3+}$  (1.14 eV versus 1.25 eV).

nanoparticles. These nanoparticles feature an energy gap of 1.25 eV between the lowest excited state ( ${}^2\text{F}_{5/2}$ ) and the ground state ( ${}^2\text{F}_{7/2}$ ) of  $\text{Yb}^{3+}$ , which lies near the triplet energy of tetracene (1.25 eV; ref. <sup>17</sup>) and above that of rubrene (1.14 eV; ref. <sup>18</sup>). When a  $\text{NaGdF}_4:\text{Yb}$ -tetracene blend film was excited at 405 nm, we recorded a strong quenching of the characteristic visible emission from tetracene in favour of a  $\text{Yb}^{3+}$  emission located at 950–1,100 nm (Fig. 3c and Supplementary Fig. 36). We observed that the emission of  $\text{Yb}^{3+}$  was strongly quenched when the blend film was exposed to air (Supplementary Fig. 37), suggesting that the  $\text{Yb}^{3+}$  emission arises from triplet-mediated energy transfer from tetracene to  $\text{Yb}^{3+}$ . Magnetic-field-dependent photoluminescence measurements showed an increase in emission from the tetracene while the emission from  $\text{Yb}^{3+}$  decreased with increasing magnetic field<sup>19,20</sup>, confirming the transfer of triplets generated by the singlet fission process to  $\text{Yb}^{3+}$  (Supplementary Figs. 44–46). By contrast, almost no quenching of the visible and no NIR emission was observed in the rubrene blend owing to inefficient triplet energy transfer to  $\text{Yb}^{3+}$ .

Figure 4a shows the photoluminescence spectra of the  $\text{NaGdF}_4:\text{Yb}$ -rubrene and  $\text{NaGdF}_4:\text{Yb}$ -tetracene blends on 980-nm excitation. Spectra corresponding to the singlet emission from both tetracene and rubrene were obtained, consistent with the upconversion of absorbed energy. This upconverted emission is visible even under ambient light conditions (Supplementary Fig. 38) and is found to have a quadratic dependence on the excitation power at low excitation fluence, followed by a slope change from 2 to 1 at higher excitation density (Supplementary Fig. 39).

Considering the broadband absorption of the  $\text{NaGdF}_4:\text{Yb}$ -rubrene blended film in the NIR wavelength region (Supplementary Fig. 40), we carried out excitation in a spectral range from 850 nm to 1,020 nm and observed upconverted emission at all excitation wavelengths (Supplementary Figs. 41, 42). These results suggest that it is the interaction between the molecular triplet exciton and the lanthanide, rather than the conventional triplet-triplet annihilation (TTA) process<sup>21–23</sup>, that mediates the upconversion process in organic molecules after triplet transfer from photoexcited  $\text{Yb}^{3+}$ -doped nanoparticles under NIR irradiation (Fig. 4b). To further investigate the upconversion mechanism, we prepared a series of blends with varying concentration ratios of  $\text{NaGdF}_4:\text{Yb}$  and rubrene or tetracene. The main emission peak shifted from 540 nm (2.29 eV) to 480 nm (2.58 eV) for the  $\text{NaGdF}_4:\text{Yb}$ -tetracene blends when the concentration ratio of tetracene to nanoparticle was changed from 10:1 to 1:100 (see Fig. 4c and Supplementary Fig. 43 for rubrene blends). Interestingly, an emission characteristic of a single tetracene molecule<sup>24</sup> was

obtained when the concentration of tetracene was diluted to 1 molecule per 100 nanoparticles. This upconverted emission is recorded at room temperature with moderate excitation density ( $<10 \text{ W cm}^{-2}$ ). This is in marked contrast to the conventional two-photon absorption methods for generating anti-Stokes emission from single molecules, which require a substantially higher excitation density ( $>10^6 \text{ W cm}^{-2}$ ). Conventional TTA upconversion through bimolecular triplet-triplet states does not enable the single molecular emission of tetracene because the emission would be shifted to lower energies due to excitonic coupling, as happens when we increase the tetracene concentration in the blend films. This again suggests that the upconverted emission is produced by a different process. Magnetic-field-dependent photoluminescence studies show no change in upconverted emission under applied magnetic field (Supplementary Fig. 47), confirming that the upconversion process is not mediated by the TTA (see Supplementary Information section 9 and Supplementary Figs. 48, 49 for full details).

Given that the singlet energy of tetracene (for a single molecule, 2.62 eV; Supplementary Figs. 48, 50) is higher than the total energy contained in two excitation photons ( $1.25 \text{ eV} \times 2 = 2.50 \text{ eV}$ ), this new mechanism enables us to obtain endothermic upconversion. To investigate this endothermic upconversion process further, we performed temperature-dependent upconversion measurements. The upconversion emission intensity for the 1:100 film gradually increased as the temperature was reduced to 80 K, presumably due to the suppression of non-radiative loss channels at low temperatures (Fig. 4d). However, further lowering the temperature resulted in a decrease in upconversion emission (Supplementary Figs. 51, 52). We note that the downshifting luminescence of the same sample under 405-nm excitation increases monotonically as the temperature drops, and the integrated emission intensity at 20 K is 12 times stronger than that measured at room temperature (Supplementary Fig. 53).

At room temperature, we measured an internal photoluminescence quantum yield (PLQY) of more than 1% for the  $\text{NaGdF}_4:\text{Yb}$ -rubrene blend film with moderate excitation of  $>16 \text{ W cm}^{-2}$ . A maximum PLQY value of  $1.9\% \pm 0.5\%$  was reached at an irradiance power density of  $75 \text{ W cm}^{-2}$  (Fig. 4e). We note that the singlet PLQY of rubrene in the blend under 405-nm excitation at room temperature was measured to be  $20\% \pm 2.1\%$ . This suggests a maximum singlet yield of about 10% per absorbed NIR photon for  $\text{NaGdF}_4:\text{Yb}$ -rubrene. A maximum PLQY value of  $16.2\% \pm 3.4\%$  was attained at 10 K (Supplementary Fig. 54), due to reduction of the non-radiative energy loss pathways at low temperatures. Given the fact that two lower-energy photons are converted to

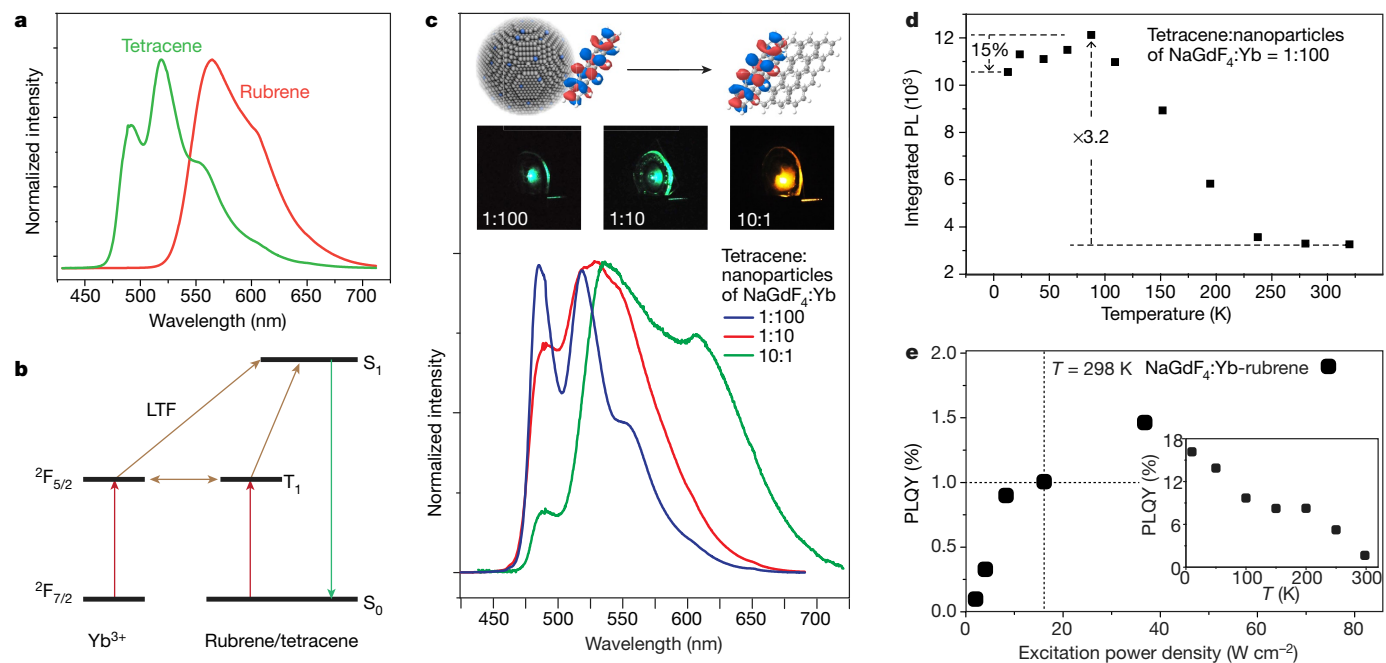


**Fig. 4 | Lanthanide-triplet excitation fusion upconversion in nanoparticle-molecule blends.** **a**, Photoluminescence spectra of NaGdF<sub>4</sub>:Yb-tetracene blend (50:1) and NaGdF<sub>4</sub>:Yb-rubrene blend (1:10) films excited at 980 nm (about 40 W cm<sup>-2</sup>), showing upconverted emission arising from the singlet state of the organics. **b**, Proposed lanthanide-triplet excitation fusion (LTF) upconversion process. **c**, Top, scheme represents the isolated molecule (left) and molecular conjugates (right) when tetracene couples with the NaGdF<sub>4</sub>:Yb nanoparticles. Note that grey and blue spheres in the nanoparticle refer to Gd<sup>3+</sup> and Yb<sup>3+</sup> ions, respectively. Bottom, upconversion spectra and corresponding emission photographs (middle) of NaGdF<sub>4</sub>:Yb-tetracene blend films with varying tetracene-to-nanocrystal ratios (1:100, 1:10 and 10:1). **d**, Plot of the

temperature-dependent upconversion emission (integrated from 475 nm to 650 nm) of the NaGdF<sub>4</sub>:Yb-tetracene blend films (tetracene: NaGdF<sub>4</sub>:Yb = 1:100). Note that PL refers to photoluminescence. Dashed arrows suggest that upconversion emission showed a 3.2-fold increase as the temperature decreased from 300 K to 80 K and then a 15% decrease when the temperature was further reduced to 10 K. **e**, The internal photoluminescence quantum yield (PLQY) of the NaGdF<sub>4</sub>:Yb-rubrene blend measured as a function of excitation power density (excitation at 980 nm). Inset, temperature-dependent quantum yield of the same sample under excitation of 980 nm for a power density of 76 W cm<sup>-2</sup>.

one higher-energy photon during the upconversion process, our system has thus converted about 32% of the absorbed photons.

In comparison with the conventional lanthanide<sup>25-28</sup>- or TTA<sup>5,22</sup>-based upconversion, a key feature of the lanthanide-triplet excitation fusion approach demonstrated here is that the excitation energy can be directly amassed in both organic and inorganic components without the need for a sensitization step. Therefore, energy loss during the sensitization process can be effectively reduced to zero<sup>29</sup>. In addition, lanthanide-doped nanoparticles have no absorption at higher energies, thereby eliminating the problem of reabsorption associated with quantum dot/molecule systems<sup>30,31</sup>. Furthermore, owing to the nature of the spin states, normal spin statistical limitations that apply to the conventional TTA do not apply to the lanthanide-triplet upconversion.

We have demonstrated that it is possible to control and manipulate triplet exciton dynamics by coupling conventional molecular systems to the unpaired spins of lanthanide ions doped in inorganic nanoparticles. Further experimental and theoretical work is required to understand the nature of the coupling in these systems. Our results open up new avenues for triplet sensitization, photocatalysis, optoelectronics, sensing, and photon frequency conversion driven by optically bright triplet excitons.

### Online content

Any methods, additional references, Nature Research reporting summaries, source data, extended data, supplementary information, acknowledgements, peer review information; details of author contributions and competing interests; and statements of data and code availability are available at <https://doi.org/10.1038/s41586-020-2932-2>.

- Bolton, O., Lee, K., Kim, H. J., Lin, K. Y. & Kim, J. Activating efficient phosphorescence from purely organic materials by crystal design. *Nat. Chem.* **3**, 205–210 (2011); correction **3**, 415 (2011).
- Baldo, M. A. et al. Highly efficient phosphorescent emission from organic electroluminescent devices. *Nature* **395**, 151–154 (1998).
- Uoyama, H., Goushi, K., Shizu, K., Nomura, H. & Adachi, C. Highly efficient organic light-emitting diodes from delayed fluorescence. *Nature* **492**, 234–238 (2012).
- Yanai, N. & Kimizuka, N. New triplet sensitization routes for photon upconversion: thermally activated delayed fluorescence molecules, inorganic nanocrystals, and singlet-to-triplet absorption. *Acc. Chem. Res.* **50**, 2487–2495 (2017).
- Schulze, T. F. & Schmidt, T. W. Photochemical upconversion: present status and prospects for its application to solar energy conversion. *Energy Environ. Sci.* **8**, 103–125 (2015).
- Ravetz, B. D. et al. Photoredox catalysis using infrared light via triplet fusion upconversion. *Nature* **565**, 343–346 (2019); correction **570**, E24 (2019).
- Mongin, C., Garakyaraghi, S., Razgoniaeva, N., Zamkov, M. & Castellano, F. N. Direct observation of triplet energy transfer from semiconductor nanocrystals. *Science* **351**, 369–372 (2016).
- Köhler, A. & Bassler, H. Triplet states in organic semiconductors. *Mater. Sci. Eng. Rep.* **66**, 71–109 (2009).
- Lamansky, S. et al. Highly phosphorescent bis-cyclometalated iridium complexes: synthesis, photophysical characterization, and use in organic light emitting diodes. *J. Am. Chem. Soc.* **123**, 4304–4312 (2001).
- Bünzli, J.-C. G. On the design of highly luminescent lanthanide complexes. *Coord. Chem. Rev.* **293–294**, 19–47 (2015).
- Klink, S. I., Kerizer, H. & van Veggel, F. C. J. M. Transition metal complexes as photosensitizers for near-infrared lanthanide luminescence. *Angew. Chem. Int. Ed.* **39**, 4319–4321 (2000).
- Penfold, T. J., Gindensperger, E., Daniel, C. & Marian, C. M. Spin-vibronic mechanism for intersystem crossing. *Chem. Rev.* **118**, 6975–7025 (2018).
- Smith, M. B. & Michl, J. Singlet fission. *Chem. Rev.* **110**, 6891–6936 (2010).
- Wykes, M., Parambil, R., Beljonne, D. & Gierschner, J. Vibronic coupling in molecular crystals: a Franck-Condon Herzberg-Teller model of H-aggregate fluorescence based on quantum chemical cluster calculations. *J. Chem. Phys.* **143**, 114116 (2015).
- Auzel, F. Upconversion and anti-Stokes processes with f and d ions in solids. *Chem. Rev.* **104**, 139–174 (2004).
- Tobita, S., Arakawa, M. & Tanaka, I. The paramagnetic metal effect on the ligand localized S<sub>1</sub>→T<sub>1</sub> intersystem crossing in the rare-earth-metal complexes with methyl salicylate. *J. Phys. Chem.* **89**, 5649–5654 (1985).

17. Tiberghien, A. & Delacote, G. Evaluation of the crystalline tetracene triplet Davydov splitting. *Chem. Phys. Lett.* **8**, 88–90 (1971).
18. Tao, S. et al. Optical pump-probe spectroscopy of photocarriers in rubrene single crystals. *Phys. Rev. B* **83**, 075204 (2011).
19. Thompson, N. J. et al. Energy harvesting of non-emissive triplet excitons in tetracene by emissive PbS nanocrystals. *Nat. Mater.* **13**, 1039–1043 (2014).
20. Tabachnyk, M. et al. Resonant energy transfer of triplet excitons from pentacene to PbSe nanocrystals. *Nat. Mater.* **13**, 1033–1038 (2014).
21. Wu, M. et al. Solid-state infrared-to-visible upconversion sensitized by colloidal nanocrystals. *Nat. Photon.* **10**, 31–34 (2016).
22. Zhao, J., Ji, S. & Guo, H. Triplet-triplet annihilation based upconversion: from triplet sensitizers and triplet acceptors to upconversion quantum yields. *RSC Adv.* **1**, 937–950 (2011).
23. Singh-Rachford, T. N. & Castellano, F. N. Photon upconversion based on sensitized triplet-triplet annihilation. *Coord. Chem. Rev.* **254**, 2560–2573 (2010).
24. Burdett, J. J., Müller, A. M., Gosztola, D. & Bardeen, C. J. Excited state dynamics in solid and monomeric tetracene: the roles of superradiance and exciton fission. *J. Chem. Phys.* **133**, 144506 (2010).
25. Zhao, J. et al. Single-nanocrystal sensitivity achieved by enhanced upconversion luminescence. *Nat. Nanotechnol.* **8**, 729–734 (2013).
26. Haase, M. & Schäfer, H. Upconverting nanoparticles. *Angew. Chem. Int. Ed.* **50**, 5808–5829 (2011).
27. Garfield, D. J. et al. Enrichment of molecular antenna triplets amplifies upconverting nanoparticle emission. *Nat. Photon.* **12**, 402–407 (2018).
28. Pollnau, M., Gamelin, D. R., Lüthi, S. R., Güdel, H. U. & Hehlen, M. P. Power dependence of upconversion luminescence in lanthanide and transition-metal-ion systems. *Phys. Rev. B* **61**, 3337–3346 (2000).
29. Nienhaus, L., Wu, M., Bulović, V., Baldo, M. A. & Bawendi, M. G. Using lead chalcogenide nanocrystals as spin mixers: a perspective on near-infrared-to-visible upconversion. *Dalton Trans.* **47**, 8509–8516 (2018).
30. Nienhaus, L. et al. Speed limit for triplet-exciton transfer in solid-state PbS nanocrystal-sensitized photon upconversion. *ACS Nano* **11**, 7848–7857 (2017).
31. Huang, Z. et al. Hybrid molecule–nanocrystal photon upconversion across the visible and near-infrared. *Nano Lett.* **15**, 5552–5557 (2015).

**Publisher's note** Springer Nature remains neutral with regard to jurisdictional claims in published maps and institutional affiliations.

© The Author(s), under exclusive licence to Springer Nature Limited 2020

### Materials

Gd(CH<sub>3</sub>CO<sub>2</sub>)<sub>3</sub>·xH<sub>2</sub>O (99.9%), Y(CH<sub>3</sub>CO<sub>2</sub>)<sub>3</sub>·xH<sub>2</sub>O (99.9%), Yb(CH<sub>3</sub>CO<sub>2</sub>)<sub>3</sub>·4H<sub>2</sub>O (99.9%), Tb(CH<sub>3</sub>CO<sub>2</sub>)<sub>3</sub>·xH<sub>2</sub>O (99.9%), Eu(CH<sub>3</sub>CO<sub>2</sub>)<sub>3</sub>·xH<sub>2</sub>O (99.9%), Lu(CH<sub>3</sub>CO<sub>2</sub>)<sub>3</sub>·xH<sub>2</sub>O (99.9%), NaOH (>98%), NH<sub>4</sub>F (99%), 1-octadecene (90%), oleic acid (90%), rubrene (99.99%), tetracene (99.99%) and all anhydrous solvents were purchased from Sigma-Aldrich. If not stated otherwise, all chemicals were used as received without further purification.

### Synthesis of 5-nm NaLnF<sub>4</sub> nanocrystals

The lanthanide nanocrystals were synthesized according to a well-documented co-precipitation method<sup>32</sup>. In a typical experiment for synthesizing 5-nm NaGdF<sub>4</sub>:Yb (50 mol%) nanocrystals, a water solution (2 ml) containing Gd(CH<sub>3</sub>CO<sub>2</sub>)<sub>3</sub> (0.2 mmol) and Yb(CH<sub>3</sub>CO<sub>2</sub>)<sub>3</sub> (0.2 mmol) was mixed with oleic acid (3.5 ml) and 1-octadecene (10.5 ml) in a 50-ml flask, followed by heating at 150 °C for 2 h. Thereafter, the reactant was cooled to 50 °C, and a methanol solution (6 ml) containing NH<sub>4</sub>F (1.36 mmol) and NaOH (1 mmol) was added. The mixed solution was stirred for 30 min. The reaction temperature was then raised to 100 °C to remove the methanol from the reaction solution. After that, the reactant was heated at 270 °C under a nitrogen atmosphere for 1 h, followed by cooling to room temperature. The resulting nanocrystals were extracted through repeated precipitation with a mixture of ethanol and methanol, collected by centrifugation at 4,000 rpm for 5 min, and re-dispersed in 4 ml of hexane. Pure NaGdF<sub>4</sub> nanocrystals were synthesized with the same procedure with the addition of the corresponding Ln(CH<sub>3</sub>CO<sub>2</sub>)<sub>3</sub> solution.

### Synthesis of NaYF<sub>4</sub> core nanoparticles

In a typical procedure<sup>32</sup>, an aqueous solution of Y(CH<sub>3</sub>CO<sub>2</sub>)<sub>3</sub>·xH<sub>2</sub>O (2 ml, 0.2 M) was mixed with 3 ml of oleic acid (OA) in a 50-ml flask. The mixture was heated at 150 °C in an oil bath for 30 min. Then 7 ml of 1-octadecene (ODE) was added to the flask. The mixture was cooled to 50 °C after 30 min. After that, a methanol solution (6 ml) containing NH<sub>4</sub>F (1.6 mmol) and NaOH (1 mmol) was added to the core precursor and stirred continuously for 30 min. After the removal of the low boiling point solvent, the temperature was increased to 290 °C under an argon atmosphere. After 2 h, the mixture was cooled down and washed with ethanol several times. The product was re-dispersed in 4 ml of cyclohexane.

### Synthesis of core-shell nanoparticles

NaLnF<sub>4</sub> shell precursor was then prepared by adding an aqueous solution of Ln(CH<sub>3</sub>CO<sub>2</sub>)<sub>3</sub>·xH<sub>2</sub>O (1 ml, 0.2 M, Ln = Y, Gd, Eu, Tb, Yb, Lu) to a mixture of OA (3 ml) and ODE (7 ml). The mixture was heated at 150 °C in an oil bath for 1 h. After cooling to 80 °C, NaYF<sub>4</sub> core nanoparticles in 4 ml of cyclohexane were added, and the resulting mixture was kept at 80 °C for 30 min. Subsequently, a methanol solution of NH<sub>4</sub>F (0.8 mmol) and NaOH (0.5 mmol) was added under magnetic stirring and kept for 30 min at 50 °C. After that, the temperature was increased to 100 °C to evaporate the low boiling point solvents. The mixture was finally heated at 290 °C under an argon atmosphere for 2 h. After cooling to room temperature, the product nanoparticles were precipitated, washed several times with ethanol, and re-dispersed in 4 ml of cyclohexane for further use.

### Preparation of ligand-free nanocrystals

The as-prepared OA-capped nanoparticles were precipitated from the hexane solution by adding acetone and were then redispersed in an acetone solution containing HCl (0.1 M). The solution was ultrasonicated for 20 min to remove the oleate ligands on the surface. After the reaction, the nanocrystals were collected by centrifugation. The precipitants were washed with acetone/methanol several times and finally redispersed in methanol<sup>33</sup>.

### Nanoparticle-molecule film fabrication

Samples were fabricated on 15-mm round glass substrates. In a typical experiment, the glass substrates were first cleaned by sequential sonication in isopropanol and acetone, followed by treatment with oxygen plasma for 10 min. The substrates were then transferred to a nitrogen glovebox. An anhydrous chloroform solution of tetracene or rubrene was mixed with the methanol solution of nanoparticles in the glovebox. The resulting nanoparticle-molecule mixed solution was drop-cast onto the glass substrates to form blend films. The as-prepared sample films were covered with a 0.13-mm thin glass slide and encapsulated with epoxy glue in the glovebox before exposure to air.

### Sample characterization

Transmission electron microscopy (TEM) measurements were carried out on a JEOL-2010F transmission electron microscope (JEOL) operating at an acceleration voltage of 200 kV. Scanning electron microscopy (SEM) images were recorded using a Leo Gemini 1530 VP SEM with an acceleration voltage of 3 kV. Ultraviolet-visible diffuse reflection spectra were recorded on a Lambda 750 spectrophotometer equipped with an integrating sphere to collect all of the diffuse reflection from the samples.

### Photothermal deflection spectroscopy

This is a highly sensitive surface-averaged absorption measurement technique. For the measurements, a monochromatic pump light beam (produced by a combination of a Light Support MKII 100 W xenon arc source and a CVI DK240 monochromator) is shone on the sample (a thin film on a quartz substrate) perpendicular to the plane of the sample, which on absorption produces a thermal gradient near the sample surface via non-radiative relaxation induced heating. This results in a refractive index gradient in the area surrounding the sample surface. This refractive index gradient is further enhanced by immersing the sample in a deflection medium comprising an inert liquid (FC-72 Fluorinert, 3M Co.) that has a high refractive index change per unit change in temperature. A fixed wavelength CW transverse laser probe beam, produced using a Qioptiq 670-nm wavelength fibre-coupled diode laser with temperature stabilizer for reduced beam pointing noise, was passed through the thermal gradient in front of the sample to produce a deflection proportional to the absorbed light at that particular wavelength. The signal is detected by a differentially amplified quadrant photodiode and a Stanford Research SR830 lock-in amplifier combination. Scanning through different wavelengths gives complete absorption spectra.

### Steady-state photoluminescence

Photoluminescence spectra were measured by exciting the solid film using a diode laser (BrixX976 NB, 980 nm, for upconversion; LDM405.100.CWA.L, 405 nm, for downshifting) with a laser spot size of about 1 mm. The spectra were recorded using a spectrometer (Andor, Shamrock SR-303i) integrated with a CCD detector (Andor, DU420A-BVF). For upconversion spectral measurements, a 900-nm short-pass filter was placed in front of the spectrometer to cut off the scattering from the laser. The magnetic field dependent photoluminescence measurements were carried out using a spectrometer (Andor, Shamrock SR-303i) integrated with a CCD detector (Andor, DU420A-BVF) with the samples placed in the centre of an electromagnet (GMW, Model 3470).

### Transient photoluminescence spectroscopy

Time-resolved photoluminescence measurements were obtained with a customized phosphorescence lifetime spectrometer (Edinburgh, FSP920-C). A nanosecond optical parametric oscillator (OPO) pumped by a 3.8-ns-pulsed Nd:YAG laser (Ekspla, NT352) was used as the excitation source. The emission from the samples was collected at an angle of 90° to the excitation beam using a pair of lenses.

## Quantum yield measurements

The quantum yield was measured using an integrating sphere method<sup>34</sup>. Samples were placed in an integrating sphere (Labsphere, 150 mm, internally coated with barium sulfate). A continuous-wave diode laser (BrixX976 NB, 980 nm) was used to excite the samples. The emission from the samples in the integrating sphere was collected by a spectrometer (Andor, Shamrock SR-303i) through an optical fibre. The signal was recorded by a CCD detector (Andor, DU420A-BVF). To avoid saturation of the detector by NIR signals, an NIR neutral density filter (Thorlabs, NENIR40B) was used to reduce the signal from the laser.

The quantum yield of upconversion emission was calculated by measuring the number of photons emitted versus the number of photons absorbed. In our quantum yield measurements, three experiments were carried out in an integrating sphere, and the total light intensity collected at the spectrometer was measured: (a) laser excitation with no sample; (b) laser excitation and sample emission with direct illumination of the sample; and (c) laser excitation and sample emission with indirect illumination of the sample. By integrating the excitation and emission signals, the upconversion efficiency was obtained as follows: the number of photons absorbed equals  $L_a A$ , where  $L_a$  is the excitation intensity in experiment (a), and  $A = 1 - (L_c/L_b)$ , where  $L_b$  and  $L_c$  are the excitation intensities in experiments (b) and (c), respectively. The number of photons emitted equals  $P_c - [(1 - A)P_b]$ , where  $P_b$  and  $P_c$  are the emission intensities in experiments (b) and (c) respectively. Thus, the quantum yield is given by  $PLQY = \{P_c - [(1 - A)P_b]\} / (L_a A)$ . This method accounts for all photons absorbed by direct excitation, indirect excitation via scattering in the integration sphere, and sample emission. Details of the quantum yield measurement and calculation can be found elsewhere<sup>34</sup>.

## Transient absorption spectroscopy

The samples were excited by a pump pulse and then probed at different delayed times using a broadband probe pulse. Transient absorption spectra were recorded over short time delays (500 fs to 6 ns) with a probe pulse covering 500–850 nm and 750–1,600 nm, and over long (1 ns to 1 ms) time delays with a probe pulse covering 350–750 nm and 850–1,020 nm. The short-time transient absorption (ps-TA) measurements were performed with a commercial transient absorption spectrometer (HELIOS, Ultrafast Systems). Part of the output from a regenerative Ti:sapphire amplifier system (Spectra Physics, Solstice, generating ultrafast pulses at about 790 nm) was used to pump a TOPAS-Prime (light conversion) to generate tunable pump pulses (355–2,600 nm). Another part of the output from this Ti:sapphire system was introduced to a YAG crystal to generate a broadband probe pulse (800–1,550 nm). The probe light is delayed using a computer-controlled piezoelectric translation stage, and a sequence of probe pulses with and without the pump is generated using a chopper wheel on the pump beam. The pump and probe pulses were focused onto a spot of area about 0.5 mm<sup>2</sup>. The time resolution of the laser pulse was about 200 fs.

In long-time transient absorption (ns-TA) measurements, an electronically controlled delay was employed. A separate frequency-doubled Q-switched Nd:YVO<sub>4</sub> laser (AOTYVO-25QSPX, Advanced Optical Technologies) is used to generate pump pulses with a temporal breadth below 1 ns at 530 nm. The pump and probe beams overlap on the sample adjacent to a reference probe beam. This reference is used to account for any shot-to-shot variation in transmission. The sample is held in a 1-mm quartz cuvette, mounted in a holder. The beams are focused into an imaging spectrometer (Andor, Shamrock SR 303i) and detected using a pair of linear image sensors (Hamamatsu, G11608) driven and read out at the full laser repetition rate by a custom-built board from Stresing Entwicklungsburo. In all measurements, every second pump shot is omitted, either electronically for long-time measurements or using a mechanical chopper for short-time measurements. The fractional differential transmission ( $\Delta T/T$ ) of the probe is calculated for each data point once 1,000 shots are collected.

In pump–probe experiments as described above, the differential transmission ( $\Delta T/T$ ) signal in the transient absorption spectra refers to features that define excited states. To identify different components from the transient absorption data, a genetic algorithm analysis was also used to distinguish different spectral species and the corresponding kinetics. In the pump–probe technique, a short light pulse (the ‘pump’) excites the sample, and the other pulse (the ‘probe’), which is broad in energy but short in time, interrogates the same spot after a time delay. The transmitted light from the probe is compared with and without the pump light and resolved by both spectral wavelength and delay time. If there is a change in the spectra of the probe because of bleaching of the ground-state transitions (‘ground-state bleach’), stimulated emission, or excited-state absorption from one excited state to another, these will manifest as a change in the transmittance of the probe,  $\Delta T$ . We recorded the signal normalized by the ground-state transmittance,  $\Delta T/T$ , to facilitate comparison across experimental configurations.

We excited CPPOA at 355 nm to create singlet excitons ( $S_1$ ) on the molecules and subsequently probed the evolution of the spectral features as a function of time. We note that the lanthanide ions have no transient absorption features and thus the entire response arises from the excited-state features of CPPOA.

## Data availability

The data underlying all figures in the main text and Supplementary Information are publicly available from the University of Cambridge repository at <https://doi.org/10.17863/CAM.59063>.

- Wang, F., Deng, R. & Liu, X. Preparation of core-shell NaGdF<sub>4</sub> nanoparticles doped with luminescent lanthanide ions to be used as upconversion-based probes. *Nat. Protoc.* **9**, 1634–1644 (2014).
- Bogdan, N., Vetrone, F., Ozin, G. A. & Capobianco, J. A. Synthesis of ligand-free colloidal stable water dispersible brightly luminescent lanthanide-doped upconverting nanoparticles. *Nano Lett.* **11**, 835–840 (2011).
- de Mello, J. C., Wittmann, H. F. & Friend, R. H. An improved experimental determination of external photoluminescence quantum efficiency. *Adv. Mater.* **9**, 230–232 (1997).

**Acknowledgements** This project received funding from the European Research Council (ERC) under the European Union’s Horizon 2020 research and innovation programme (grant agreement no. 758826) and from Marie Skłodowska-Curie grant agreements nos 797619 (TET-Lanthanide project), 748042 (MILORD project) and 646176 (EXTMOS project). We acknowledge support from the Engineering and Physical Sciences Research Council (EPSRC) and the Winton Programme for the Physics of Sustainability, the Singapore Ministry of Education (grant MOE2017-T2-2-110), the Singapore Agency for Science, Technology and Research (grant A1883c0011), and the National Research Foundation, Prime Minister’s Office, Singapore under the NRF Investigatorship programme (award no. NRF-NRFI05-2019-0003). R.D. acknowledges support from the National Natural Science Foundation of China (grant 51872256) and the Zhejiang Provincial Natural Science Foundation of China (grant LR19B010002). Computational resources were provided by the Consortium des Équipements de Calcul Intensif (CÉCI), funded by the Fonds de la Recherche Scientifique de Belgique (FRS-FNRS) under grant no. 2.5020.11, and by the Tier-1 supercomputer of the Fédération Wallonie-Bruxelles, which is infrastructure funded by the Walloon Region under grant agreement no. 1117545. L.N. acknowledges support from the Jardine Foundation. J.Z. thanks the China Scholarship Council for a PhD scholarship (no. 201503170255). S.A. acknowledges financial support from DST-UKIERI (DST/INT/UK/P-167/2017) and SERB-ECRA (ECR/2018/002056).

**Author contributions** S.H., R.D. and A.R. designed the experiments. S.H., R.D., Z.Y. and B.Z. performed nanocrystal synthesis and film preparation. S.H., R.D., L.N., U.H., A.S. and S.A. carried out spectroscopic measurements. S.H., Q.G. and J.Z. contributed to transient absorption experiments and data analysis under the supervision of A.B. and A.R. H.T., A.P. and D.B. carried out theoretical calculations. H.X. prepared organic molecules. Z.H. prepared tetracene derivatives under the supervision of M.L.T. M.A.-J. and A.S. performed PDS measurements. S.H., R.D., X.L. and A.R. wrote the manuscript. X.L. and A.R. supervised the project. All authors discussed the results and commented on the manuscript.

**Competing interests** The authors declare no competing interests.

## Additional information

**Supplementary information** is available for this paper at <https://doi.org/10.1038/s41586-020-2932-2>.

**Correspondence and requests for materials** should be addressed to R.D., X.L. or A.R.

**Peer review information** Nature thanks Jiajia Zhou and the other, anonymous, reviewer(s) for their contribution to the peer review of this work.

**Reprints and permissions information** is available at <http://www.nature.com/reprints>.